Vertically Integrated Visible and Near-Infrared Metasurfaces Enabling an Ultra-Broadband and Highly Angle-Resolved Anomalous Reflection

Song Gao,[†] *Sang-Shin Lee,*[*,†] *Eun-Soo Kim,*[†] *and Duk-Yong Choi*[‡]

[†]Department of Electronic Engineering, Kwangwoon University, 20 Kwangwoon-ro, Nowon-gu, Seoul 01897, South Korea

[‡]Laser Physics Centre, Research School of Physics and Engineering, Australian National University, Canberra ACT 2601, Australia

KEYWORDS: vertically integrated metasurface, broadband anomalous deflection, high angular dispersion, spectrum splitting, polarization beam splitter

ABSTRACT:

An optical device with minimized dimensions, which is capable of efficiently resolving an ultra-broad spectrum into a wide splitting angle but incurring no spectrum overlap, is of importance in advancing the development of spectroscopy. Unfortunately, this challenging task cannot be easily addressed through conventional geometrical or diffractive optical elements. Herein, we propose and demonstrate vertically integrated visible and near-infrared metasurfaces which

render an ultra-broadband and highly angle-resolved anomalous reflection. The proposed metasurface capitalizes on a supercell that comprises two vertically concatenated trapezoid-shaped aluminum antennae, which are paired with a metallic ground plane via a dielectric layer. Under normal incidence, reflected light within a spectral bandwidth of 1000 nm ranging from λ = 456 nm to 1456 nm is efficiently angle-resolved to a single diffraction order with no spectrum overlap via the anomalous reflection, exhibiting an average reflection efficiency over 70% and a substantial angular splitting of 58°. In light of a supercell pitch of 1500 nm, to the best of our knowledge, the micron-scale bandwidth is the largest ever reported. It is noted that the substantially wide bandwidth has been accomplished by taking advantage of spectral selective vertical coupling effects between antennae and ground plane. In the visible regime, the upper antenna primarily renders an anomalous reflection by cooperating with the lower antenna, which in turn cooperates with the ground plane and produces phase variations leading to an anomalous reflection in the near-infrared regime. Misalignments between the two antennae have been particularly inspected to not adversely affect the anomalous reflection, thus guaranteeing enhanced structural tolerance of the proposed metasurface.

The metasurface has attracted a great deal of attention as a prominent emerging technology to pave the way for the development of a variety of ultrathin nanophotonic components/modules, including the anomalous light deflector,[1,2] lens,[3,4] waveplate,[5,6] hologram,[7,8] and vortex beam generator.[9,10] In addition to the control of light propagating in free space, the metasurface has also been applied to optical waveguides to embody integrated functional devices.[11-14] In consideration of the light wavefront that may be efficiently tailored via a space-variant phase profile, the metasurface is capable of creating the phase profile on a planar surface over a

subwavelength scale, while traditional optical components resort to phase shift accumulated over a long propagation distance. In particular, taking into account that a supercell associated with a metasurface may be constructed to produce a constant phase gradient, where the phase varies with the position in a linear fashion over a span of 2π, the laws of refraction and reflection have been rewritten to account for the phenomenon of anomalous light deflection.[1]

A reflective metasurface, exploiting a metal-dielectric-metal (MDM) configuration based on gap-plasmon resonance, garnered enormous attention and functioned as a broadband anomalous reflector operating in the near-infrared (NIR) spectral band.[2] For the elemental supercell constituting the metasurface, the linearly varying 2π-phase shift underpinning the anomalous reflection has been derived from a suite of discrete antennae with varying lateral dimensions. The use of discrete antennae in the metasurface may pose a challenge in fabrication when it comes to the visible (VIS) band as the geometrical dimension of each element becomes substantially small. A single trapezoid-shaped antenna in place of the discrete antenna array might be used to facilitate the fabrication of the delicate device structure.[15-19] The scheme capitalizing on such a single antenna is expected to provide an enhanced phase gradient over a wide band, thereby rendering broadband anomalous reflection. For the supercell with a superwavelength lattice period, the angle of anomalous reflection is simply determined by the modified diffraction equation.[17] Unlike conventional blazed gratings, which tap into a sawtooth échelette profile to exhibit a maximum diffraction efficiency at a specific wavelength, the anomalous reflection is efficiently achieved throughout a broad band for the planar metasurface.[15,16] It is noted that due to the inherent shape of the antenna, the enhanced anomalous reflection is polarization-dependent and therefore the metasurface can be potentially treated as a broadband polarization beam splitter,[15] which might not be easily fulfilled using a

diffraction grating.[20] Despite its vulnerability to dissipative optical loss, a plasmonic metasurface is deemed to give rise to an appreciable level of anomalous reflection beyond 80%, which can readily be applied to spectroscopy, imaging, and photovoltaics.[15,21] Besides the trapezoid-shaped antenna, a quasi-continuous metasurface resorting to an optical catenary was studied.[22]

An optical device, which exhibits a minimized dimension yet a capability of widely angle-resolving an ultra-broad spectrum, is of importance and highly desirable in developing spectroscopic instruments and therefore advance the related fields. For the metasurface, the spectra pertaining to the anomalous reflection under normal incidence are fundamentally limited to no more than the pitch of the superwavelength lattice. The demonstrated bandwidth of concern has been constrained to a few hundreds of nanometres, corresponding to only a small fraction in the middle of the spectrum.[15,17] The metasurface could be scaled up by appropriately enlarging the supercell lattice so that the achievable band could be accordingly increased. However, this method entails a low angular dispersion of the anomalous reflection and usually results in a red-shift of the operation band towards the long wavelength region while light at shorter wavelength will be funnelled into several undesired diffraction orders, incurring severe spectrum overlap and consequently extra filters are essentially required for practical usage.[16] The bandwidth should be limited because the phase gradient for creating efficient anomalous reflection, which is associated with the resonance response, cannot be fulfilled over an ultra-broadband by virtue of a single antenna.[23,24] Instead of simply optimizing the lateral dimensions of the antenna, which rarely contributes to the broadening of the spectra but mostly incurs their shift, a planar arrangement of various shapes of nanoantennae is anticipated to be a prime candidate for the implementation of a metasurface operating at multiple discrete wavelengths.[19,25] However, the metasurface with a dielectric of fixed thickness is not suitable for simultaneously rendering

highly efficient anomalous reflection at far-spaced wavelength regions.[26] The metasurface, inclusive of segments that are responsible for distinct wavelength regions, is deemed to be limited in efficiency, due to its diminished effective metasurface area for each wavelength region. Such a metasurface is not a recommendable candidate to attain both high efficiency and broad band.[27] An off-axis illumination method could be adopted to potentially mitigate this issue.[28]

A distinguished alternative to expand the bandwidth is a configuration of stacking, which has been incorporated to realize ultra-broadband perfect absorbers, where lightwave spectral bands are absorbed at the corresponding depths of the structure.[29,30] Recent years also witnessed growing interest in applying the configuration to metasurfaces, which are mostly operated in transmission mode,[31-35] except for a couple of theoretical works in relation to the reflection-mode operation.[26,36,37] Especially for the transmissive metasurface, one usually needs to cascade more antenna layers in order to expand the operation bandwidth.[38] The reflective metasurface is comprised of multilayered antenna arrays sharing a metallic ground plane. Such design strategy enables the arbitrary wavefront manipulation in individual spectral bands. As an application for light bending, the device is required to substantially quench an unwanted coupling between the vertically cascaded antenna arrays, providing anomalous reflection of about 60% efficiency at λ = 700 nm and 1055 nm.[26] Metasurfaces counting on a geometric phase also feature a broadband operation, yet their operation is mostly restricted to circularly polarized light.[39]

In this paper, an ultra-broadband and highly angle-resolved anomalous reflection is realized resorting to vertically integrated visible and near-infrared metasurfaces. The supercell constituting the proposed metasurface consists of two vertically integrated aluminum (Al) antennae of a trapezoidal shape, which are paired with a metallic ground plane via a dielectric layer. In the NIR regime, the lower antenna, which is immersed in the dielectric layer, is

supposed to cooperate with the ground plane, and produce phase variations that lead to efficient anomalous reflection. In the VIS regime, the upper metallic antenna at the top primarily cooperates with the embedded antenna, which effectively serves as a reflecting ground plane, thereby rendering efficient anomalous reflection. In this way, the proposed metasurface is drastically advanced in terms of the spectral bandwidth incurring no spectrum overlapping. The underlying principle of operation is rigorously studied through the inspection of diffraction characteristics, in tandem with electromagnetic field profiles. A suite of devices was manufactured and evaluated to successfully verify the claimed highly angle-resolved anomalous reflection across the ultra-wideband encompassing the VIS and NIR regimes.

Fig. 1a shows a schematic of the proposed metasurface, where two different trapezoid-shaped antennae in Al are vertically cascaded and separated via a dielectric layer made of SiO_2 from an optically thick Al substrate, which acts as a reflecting ground plane. Al is particularly selected due to its compatibility with the cost-effective complementary metal-oxide-semiconductor process.[40] Fig. 1b shows that the two Al antennae constituting a supercell are designed in such a way that the lengths are identical while the bases exhibit dissimilar subwavelength dimensions in width. The upper and lower trapezoids are denoted the top VIS-antenna and the embedded NIR-antenna, respectively. In the presence of the embedded NIR-antenna, the dielectric region is divided into upper and lower SiO_2 layers. The morphology of the upper SiO_2 layer replicates that of the embedded NIR-antenna when no planarization process is involved during its deposition.[41] Taking this into account, the upper SiO_2 layer has been designed in a trapezoidal shape. The supercells comprising the antenna array are meticulously arranged in accordance with pitches of P_x = 1500 nm and P_y = 250 nm. The base widths of the antennae are w_1 = 90 nm, w_2 = 250 nm, w_3 = 40 nm, and w_4 = 130 nm. More detailed structural parameters are

described in the figure captions. A supercell based on a single layer of trapezoid-shaped antenna whose width is continuously varying is known to allow for successive gap-plasmonic resonances along the longitudinal direction, in collaboration with a bottom ground plane.[15-17] For incident light interacting with progressive resonance variations in terms of the amplitude and phase, a dispersive phase gradient is induced within the supercell along the longitudinal direction of the space-variant antenna, resulting in a broadband anomalous reflection.[15] According to the consistency between the generalized laws of reflection and diffraction, the angle of anomalous reflection matches that of the first order diffraction,[42-44] connoting that for the case of normal incidence, the entire operation spectra for the anomalous reflection are limited below the lattice period (P_x). The propagation direction for the anomalously reflected light can be predicted by noting the interfacial phase shift, which gradually increases along the axis from the narrow to the wide side of the antenna (in our case, the negative 1st order diffraction). The performance of the proposed metasurface has been investigated by conducting simulations with the assistance of a commercial tool based on the finite difference time domain domain (FDTD) method (FDTD Solutions, Lumerical, Canada).[45]

Fig. 1c shows that for normally incident light with the electric field aligned parallel to the y-axis, the proposed metasurface is theoretically assessed in terms of the anomalous reflection spectrum corresponding to the -1st order diffraction. It is observed that the spectrum exhibits double peaks centered around λ = 600 nm and λ = 1300 nm in the VIS and NIR bands, respectively. The efficiency, reaching a global maximum of 82%, surpasses 50% over a spectral bandwidth of $\Delta\lambda$ = 1000 nm running from 456 nm to 1456 nm. The corresponding reflection angle ranges from 18° to 76° with an average diffraction efficiency of 71%. When the upper limit of the operation wavelength, which is set by the lattice period of P_x = 1500 nm, is taken into

account, with the UV band below 400 nm being excluded, the bandwidth allowing for an enhanced anomalous reflection is found to occupy as much as 91% of the spectrum in accordance with the relationship of $\Delta\lambda$ / (P_x - 400). To the best of our knowledge, the micron-scale operation bandwidth leading to a highly angle-resolved anomalous reflection, spanning the VIS and NIR band, is noteworthy in light of the dimensions of the supercell. Furthermore, the efficiency of our proposed metasurface tops 60% throughout the bandwidth of $\Delta\lambda$ = 940 nm ranging from λ = 490 nm to 1430 nm, which is certainly superior to the previous work that only enables the anomalous reflection with similar efficiency in two discontinuous bands.[26] In addition, the achievable bandwidth is nearly double that of the metasurface resorting to a single antenna. Simply optimizing the structural parameters, such as the length and base widths of the antenna, and the thickness of the dielectric layer, can rarely significantly enhance the bandwidth for a metasurface incorporating a single antenna. Related discussions are included in Fig. S1 of the ESI.† Therefore, the proposed metasurface obviously exhibits conspicuous features, including extremely large bandwidth, in combination with high efficiency and high angular dispersion. Another aspect deserving more recognition is the efficiency for relatively large reflection angles. For most of the conventional broadband metasurfaces, the deflection efficiency typically drops below 30% for an angle of 70°.[15,16] By means of the inverse free-form design for an example, the efficiency can improve up to 70%.[46-48] Degradation in the efficiency for large reflection angles is chiefly imputed to an impedance mismatch at the metasurface interface.[49] For conventional metasurface designs, the discrete antennae constituting the elemental supercell of the metasurface are deemed to impart a linear phase variation along the longitudinal direction, providing a local reflection coefficient equivalent to unity at each point. The selection of each discrete antenna satisfying the requirement is fulfilled through a uniform array of identical

elements that only invokes normal reflection. Under normal incidence, the wave impedances for both incident ($\eta_0 / \cos\theta_i$) and reflected ($\eta_0 / \cos\theta_r$) light are assumed to be tantamount to that of free space, where η_0 is the wave impedance in free space; θ_i and θ_r are the angles of incidence and reflection, respectively ($\theta_r = \theta_i = 0$ in this case). Nevertheless, for the metasurface that enables an anomalous reflection ($\theta_i = 0$, $\theta_r \neq 0$), the wave impedance of the reflected light has been modified. The mismatched impedances inevitably cause light energy to funnel into several diffraction orders. Accordingly, the anomalous reflection efficiency as a function of the reflection angle can be calculated as $4\cos(\theta_r)/(1+\cos(\theta_r))^2$ and consequently the efficiency for the angle of 70° might be no more than 76%, as indicated by the "star" mark in Fig. 1c for the case of no loss.[49,50] Our metasurface is presumed to provide a decent efficiency of 65% at λ = 1410 nm, benefitting from the ultra-broadband feature. It should be noted that a high anomalous reflection efficiency might be demonstrated at moderate reflection angles through the realization of a linear phase gradient in the conventional metasurface which exploits discrete antennae, considering the metasurface suffers from no notable wave impedance mismatch between the normally incident light and obliquely reflected light. However, a nonlinear phase gradient should be taken into account so as to compensate for the impedance mismatch corresponding to large reflection angles, from the perspective of enhancing the efficiency.[49]

The proposed metasurface has been elaborately designed to improve the performance as follows. For the top VIS-antenna, the widths need to be minimized to a certain extent so that the blockage of the NIR reflection that is associated with the embedded NIR-antenna could be alleviated, while the widths should be sufficiently enlarged to facilitate anomalous reflection in the VIS band. The design of the lateral dimensions of the top VIS-antenna is addressed in Fig. S2 in the ESI.† As a result, the base width w_4 of the top VIS-antenna is determined to be 130 nm.

The embedded NIR-antenna is properly designed to have a length of 1000 nm, in an attempt to enable highly efficient anomalous reflection and minimize the specular reflection in the NIR regime. The top VIS-antenna in tandem with the embedded NIR-antenna is designed to exhibit the same length, thereby preventing the specular reflection of VIS light from the embedded NIR-antenna. Influence of the antenna length is described in Fig. S3 of the ESI.† When it comes to the upper SiO_2 layer sandwiched between the two Al antennae, its thickness should be considered a crucial factor that determines the efficiency in the VIS band. Fig. 2 shows that the device performance has been scrutinized for the cases of (a) the proposed metasurface incorporating the VIS-antenna in tandem with the NIR-antenna, (b) a metasurface with the embedded NIR-antenna alone, and (c) a metasurface with the top VIS-antenna alone, for the upper-SiO_2 thicknesses of (i) h = 30 nm, (ii) h = 60 nm, and (iii) h = 90 nm. The role of the top VIS-antenna is expounded by examining the -1st order diffraction spectra (in solid lines) in Fig 2a and 2b. For a constant thickness of upper SiO_2, the spectral responses for beyond λ = 900 nm are approximately independent of the existence of the VIS-antenna, signifying that the VIS-antenna is almost transparent from the viewpoint of the incident NIR light, and rarely poses a significant threat to the functioning of the embedded NIR-antenna. Fig. 2b shows that for the metasurface exploiting only the embedded NIR-antenna, the NIR diffraction characteristics are examined to exhibit slight red-shift depending on the upper SiO_2, which helps increase the operation bandwidth, and improves the efficiency for large angles of reflection. The red-shift relating to the gap-plasmonic resonance might be attributed to the induced upper SiO_2 preferentially storing mode energy in the dielectric layer, which implies an increased effective refractive index of the resonance mode.[51]

Fig. 2a(i) through 2a(iii) show that for our metasurface, the thickness of the upper SiO_2 is mainly accountable for the anomalous reflection in the VIS band. The corresponding efficiency is boosted by increasing the thickness from 30 nm to 60 nm. However, further increase in the thickness greater than 90 nm is liable to adversely affect the efficiency. A similar phenomenon is observed in the case of the metasurface drawing upon a top VIS-antenna that is linked to a perfect metal ground via the same upper SiO_2 (Fig. 2c), indicating that the bottom MDM structure based on the embedded NIR-antenna may effectively serve as a reflector. It is understood that the absorption level and the phase tuning range particularly hinge on the dielectric thickness.[49] Fig. 2a and 2c plot in black dashed lines the total reflection, which is accounted for by the level of absorption. For a small dielectric thickness like h = 30 nm, an entire phase tuning of up to 2π is readily attained for the anomalous reflection in the VIS band. However, the reflection tends to decline rapidly as a result of worsened metallic loss. Although a thicker dielectric layer like h = 90 nm is useful for overcoming the absorption, the phase tuning range for the supercell unavoidably diminishes, which in turn lowers the anomalous reflection. The normal reflection will be accordingly reinforced, as indicated by the blue dashed line in Fig. 2a(iii). For a gap-plasmonic metasurface incorporating a single metallic antenna with various dielectric thicknesses, the phase shift for VIS light is calculated with respect to the antenna width. The results are shown in Fig. S4 of the ESI, indicating that the phase shift increases with decreasing thickness of the dielectric layer.† The anomalous reflection can be optimized throughout the VIS band by employing a moderately thin dielectric thickness, such as h = 60 nm. As shown in Fig. 2a(ii), the anomalous reflection surpasses 50% for the spectral bandwidth of over 1000 nm ranging from λ_{min} = 417 to λ_{max} = 1420 nm, with the normal reflection remaining below 2.2% in the band running from 400 nm to 1304 nm. The same -1st order diffraction

efficiency in the VIS band ranging from λ = 430 nm to 742 nm is particularly depicted in Fig. S5 of the ESI, which stably exceeds 60%.† The lower limit of the operation wavelength apparently blue shifts as the dielectric thickness decreases from 90 nm to 60 nm. It should be noted that for a conventional diffraction grating, the free spectral range defines the largest bandwidth in a given order which does not overlap the same bandwidth in an adjacent order and is usually characterized as $\lambda_{max} - \lambda_{min} = \lambda_{min}/m$, where m indicates the diffraction order.[52] As in our case, m = 1 and λ_{min} = 417 nm, the operation wavelength up to which no spectrum overlap can be incurred is limited to λ_{max} = 834 nm. An extraordinary result is observed from our metasurface that the upper wavelength is greatly extended to 1420 nm. For the proposed metasurface, the simulated averaged maximum efficiency in both second and third diffraction orders between λ = 400 nm and 500 nm is 1.3% (not shown here). The estimated evolution of the reflected light into the anomalous reflection mode gives rise to an efficiency surpassing 95% (ratio of the anomalous reflection to the total reflection) in the wavelength range of 497 nm to 1304 nm, as shown in Fig. S6 in the ESI.† The thicknesses of the upper and the lower SiO_2 dielectrics are determined to be unequal, with a view to simultaneously obtaining the maximum efficiency in the VIS and NIR band. From the perspective of broadening the bandwidth, a co-planar arrangement of the two antennae is therefore not recommended (detailed results shown in Fig. S7 of the ESI).†.

Fig. 3 shows that the total electric field distributions on the surfaces of the two Al antennae, which have been inspected for our metasurface with an upper SiO_2 layer of 60-nm thickness. Fig. 3a shows that at the wavelength of 520 nm, the top VIS-antenna presents a stronger radiative resonance than the embedded NIR-antenna. As the wavelength increases, the resonance position for the top VIS-antenna progressively moves towards the side with larger widths of Al, and the embedded NIR-antenna starts to take effect, as implied in Fig. 3b and 3c. Fig. 3d shows that the

electromagnetic field for the NIR light at λ = 1100 nm is primarily localized in the vicinity of the embedded antenna. Fig. 3e and 3f explore the electric (E) and magnetic (H) field profiles on the specified cross-sectional planes for two representative wavelengths of 520 nm and 1100 nm, respectively, with the intention of concretely confirming the nature of gap-plasmonic resonance. The excitation of the resonance mode for the wavelength of 520 nm (1100 nm) is supported by the reinforced magnetic field in connection with the upper (lower) SiO_2 layer alongside the strengthened electric field on either side of the top VIS-antenna (embedded NIR-antenna), which signifies the development of an antiparallel electric-displacement current at the metal-dielectric interfaces, as indicated by the white arrows.[17] It should be noted that the mode energy at long wavelength is partially channelled to the top SiO_2 layer, which is in accordance with the explanation of the red-shift effect in the diffraction spectrum in Fig. 2b. These results reveal that the top and embedded antennae are in charge of the anomalous reflection in the VIS and NIR spectral band, respectively. The crucial mechanism underlying the proposed device, which resembles a broadband perfect absorber, is essentially differentiated from the conventional devices, wherein the vertical couplings between the multilayer antenna arrays are prohibited.[26,36] The spectral bandwidth is presumed to be potentially ameliorated by vertically integrating more antennae.

The broadband feature can be obtained for the metasurface with an upper dielectric layer thickness of h = 90 nm or h = 60 nm. However, at large reflection angles such as -70°, the upper dielectric layer of 60-nm thickness gives a simulated anomalous reflection efficiency of 52%, which is somewhat lower than 65% for the case of 90-nm thickness. For the purpose of realizing both broadband and high efficiency at large reflection angels, we chose to fabricate the metasurface with an upper SiO_2 thickness of 90 nm rather than 60 nm. As depicted in Fig. 4, the

proposed metasurface was manufactured through two-step lift-off processes, in combination with highly accurate overlay alignment in the electron beam lithography (EBL) process. A positive electron-beam resist of ZEP520A was initially spin-coated on top of the SiO_2 layer, then the first trapezoidal patterns for the embedded NIR-antenna were exposed with an EBL system (RAITH 150) and developed in n-amyl acetate. A 40-nm thick Al film was subsequently deposited by an electron-beam evaporator (Temescal BJD-2000). When the resist was completely removed by means of a ZEP remover (ZDMAC) via the first step of the lift-off process, the first trapezoidal antenna in Al was created. The construction of the top structures, such as the upper SiO_2 and the top trapezoidal Al for the VIS-antenna, follows the same procedure mentioned above, or processes (vi) through (x). The upper SiO_2 layer in process (vi) is deposited via plasma-enhanced chemical vapour deposition (Plasmalab 100, Oxford). During the process, we noticed that the shape of the embedded trapezoidal Al was modified at a deposition temperature of 250 ^{o}C; hence, the temperature was kept below 200 ^{o}C. The completed metasurface occupies a footprint of 20 μm × 20 μm. A high-resolution scanning electron microscope (SEM) image of the top view of the fabricated sample shows two precisely arranged trapezoids, exhibiting a misalignment of as small as 30 nm.

To experimentally validate the claimed performance of the proposed device, its far-field intensity profile was recorded in terms of the wavelength and the reflection angle. A Fourier-transform-based angle-resolved spectroscopy (FT-ARS) measurement was carried out to permit the characterization at small diffraction angles. Although the measurement system equipped with a microscope objective having a numerical aperture of 0.87 guarantees a relatively large collection angle of 60°, the measurement data from the system are incomplete because the spectrum of the light source is restricted from 400 nm to 900 nm (corresponding to reflection

angles from 15.5° to 34.5°). For the execution of the NIR measurement over the spectral band of λ = 900 nm to 1450 nm, we utilized a custom-built test setup (see the Fig. S8 in ESI for details).† It is presumed that the NIR far-field intensity distributions in accordance with the reflection angles scanning from -35° to +35° are not practically available, since the incident light is intercepted by the detector. It has been concretely corroborated that the suggested metasurface is able to render an enhanced anomalous reflection into a single diffraction order across an ultra-broadband that encompasses the VIS and NIR regimes. Fig. 5a shows the measurement results which correlate well with the simulation results in Fig. 5b. The desired anomalous reflection surpasses 50% not only in the VIS band of λ = 440 nm to 780 nm, but in the NIR band of λ = 964 nm to 1300 nm as well, assuming double peaks positioned around λ = 550 nm and 1150 nm, with efficiencies of ~72% and 85%, respectively. In addition, no higher diffraction orders are found in the shorter wavelength range. Since the fabricated device is designed with an upper SiO_2 thickness of 90 nm rather than 60 nm, in addition to the desired anomalous reflection, part of the visible light energy is channelled into the zero-diffraction order, as can be expected from the simulation result in Fig. 2a(iii). The discrepancy between the measurement and simulation outcomes, including the decreased efficiency and the slight shift of the wavelengths corresponding to the maximum efficiency, is judged to stem from fabrication imperfections, such as surface/edge roughness of the Al structure, and deviations in the realized dimensions. In addition, the spectrometer used for the FT-ARS measurement is susceptible to tenuous sensitivity in the proximity of λ = 850 nm, which possibly brings about the discrepancy of the efficiency in the wavelength range of 800 to 900 nm. The anomalous reflection efficiency at the reflection angle of as large as -70° is measured to be 23%, which is lower than the simulated

value. Nonetheless, a reflection of 50% is still observed at the relatively large angle of -60° (λ = 1300 nm), which is comparable with that of previous works.[46,48]

When it comes to the design based on a cascaded configuration, misalignment between different layers practically comes into play. In an effort to explore the dependence of the anomalous reflection on the degree of misalignment, a set of devices was prepared to entail a controlled 100-nm misalignment along the x- and y-directions. Despite the misalignment, the measured far-field intensity profiles in the VIS band remain stable except for minor deteriorations especially for the misalignment along the x-direction, as shown in Fig. S9 of the ESI.† The measurement results are in good agreement with the simulation results that are elucidated in Fig. S10 of the ESI.† Since the actual fabricated sample with the deliberately introduced misalignment cannot be readily simulated due to its complicated shape, a flat upper SiO_2 layer is considered for simulations. In the case of a simulated metasurface incorporating a flat upper SiO_2 layer, the efficiency is hardly influenced by the y-misalignment throughout the whole spectral band. The VIS band efficiency is slightly sensitive to the x-misalignment, which is most likely because the progressively evolving resonance mode profile of the top VIS-antenna is gradually distorted and consequently suppresses the visible anomalous reflection. Nevertheless, there is no serious fluctuation in the efficiency caused by the relatively large misalignment, guaranteeing the high structural tolerance of the proposed integrated metasurface.

An ultra-broadband and highly angle-resolved anomalous reflection is successfully accomplished by capitalizing on vertically integrated VIS and NIR metasurfaces. We envision that the operation bandwidth can be further extended by integrating more antennae. As described in Fig. S11(a) of the ESI, placing another thinner trapezoid-shaped Al antenna on the designed metasurface blue-shifts the lower limit of the operation wavelength further into the UV region.†

Without sacrificing the efficiency in the long wavelength bands, the efficiency exceeds 50% through a spectral bandwidth of $\Delta\lambda$ = 1088 nm from 374 nm to 1462 nm. The scheme of vertical cascading can be also engineered to build numerous versatile metasurfaces; for instance, Fig. S11(b) of the ESI shows that light can be anomalously reflected in the opposite directions by reversing the orientation of the top VIS-antenna.† This idea can be efficiently leveraged to embody directional spectrum splitters and photovoltaic devices.[19, 53,54]

Vertically integrated VIS and NIR metasurfaces capitalizing on a pair of concatenated trapezoid-shaped Al antennae were developed and characterized. The reflected light was highly angle-resolved via an anomalous reflection to a single diffraction order without spectrum overlap over an ultra-wide spectral bandwidth of 1000 nm, spanning the VIS and NIR regimes. Benefiting from the conspicuous feature of the ultra-broad bandwidth, the anomalous reflection is anticipated to retain a high efficiency of 65% at the large reflection angle of -70°. The operation bandwidth of the designed metasurface is nearly double that of a conventional metasurface employing a single antenna. Diffraction spectra in conjunction with electromagnetic field distributions were systematically inspected to assist the comprehension of the underlying principle of the ultra-broadband anomalous reflection. It was discovered that the vastly broadened operation bandwidth is primarily ascribed to the spectral selective vertical coupling effect between the two cascaded Al antennae and the ground plane. Pronounced structural tolerance of the proposed metasurface was finally confirmed by examining the effect of misalignments between layers on the anomalous reflection, both in measurement and in simulation. It is anticipated that the demonstrated device could be readily applied to a wide range of applications that include ultra-broadband spectrometers, polarization beam splitters, thin film solar cells, and spectral imaging.

†Electronic Supplementary Information (ESI) available: Detailed information of the top VIS-antenna design, discussion of the conversion efficiency, effect of misalignment, additional experimental results, comparison with other metasurface design, as well as versatile metasurface designs.

AUTHOR INFORMATION

Corresponding Author
* E-mail: slee@kw.ac.kr

ORCID

Song Gao: 0000-0001-9410-3040

Sang-Shin Lee: 0000-0001-5686-4893

Duk-Yong Choi: 0000-0002-5339-3085

Notes

The authors declare no competing financial interest.

ACKNOWLEDGMENT

This work was supported by the National Research Foundation of Korea (NRF) grants funded by the Korea government (MSIP) (Nos. 2016R1A2B2010170 and 2011-0030079) and by a Research Grant of Kwangwoon University in 2018. The work was partly supported by the Australian Research Council Future Fellowship (FT110100853, Dr. Duk-Yong Choi), and was performed in part at the ACT node of the Australian National Fabrication Facility. The authors thank Prof. L. Shi, Prof. J. Zi and Y. Zhang from Fudan University and Dr. H. Yin from Ideaoptics Inc., for their help with the Fourier-transform-based angle-resolved spectroscopy (FT-ARS) measurements.

REFERENCES

(1) N. Yu, P. Genevet, M. A. Kats, F. Aieta, J.-P. Tetienne, F. Capasso and Z. Gaburro, Science, 2011, 334, 333-337.
(2) S. Sun, K.-Y. Yang, C.-M. Wang, T.-K. Juan, W. T. Chen, C. Y. Liao, Q. He, S. Xiao, W.-T. Kung, G.-Y. Guo, L. Zhou and D. P. Tsai, Nano Lett., 2012, 12, 6223.

(3) M. Khorasaninejad, W. T. Chen, R. C. Devlin, J. Oh, A. Y. Zhu and F. Capasso, Science, 2016, 352, 1190.
(4) A. Arbabi, Y. Horie, M. Bagheri and A. Faraon, Nat. Nanotechnol., 2015, 10, 937.
(5) F. Ding, Z. Wang, S. He, V. M. Shalaev and A. V. Kildishev, ACS Nano, 2015, 9, 4111.
(6) Z. H. Jiang, L. Lin, D. Ma, S. Yun, D. H. Werner, Z. Liu and T. S. Mayer, Sci. Rep., 2014, 4, 7511.
(7) G.Y. Lee, G. Yoon, S.-Y. Lee, H. Yun, J. Cho, K. Lee, H. Kim, J. Rho and B. Lee, Nanoscale, 2018, 10, 4237.
(8) K. Huang, Z. Dong, S. Mei, L. Zhang, Y. Liu, H. Liu, H. Zhu, J. Teng, B. Luk'yanchuk, J. K. W. Yang and C.-W. Qiu, Laser Photonics Rev., 2016, 10, 500.
(9) Y. Yang, W. Wang, P. Moitra, I. I. Kravchenko, D. P. Briggs and J. Valentine, Nano Lett., 2014, 14, 1394.
(10) F. Yue, D. Wen, J. Xin, B. D. Gerardot, J. Li and X. Chen, ACS Photonics, 2016, 3, 1558.
(11) D. Ohana, B. Desiatov, N. Mazurski and U. Levy, Nano Lett., 2016, 16, 7956.
(12) D. Vercruysse, P. Neutens, L. Lagae, N. Verellen and P. V. Norpe, ACS Photonics, 2017, 4, 1398.
(13) Z. Li, M.-H. Kim, C. Wang, Z. Han, S. Shrestha, A. C. Overvig, M. Lu, A. Stein, A. M. Agarwal, M. Loncar and N. Yu, Nat. Nanotechnol., 2017, 12, 675.
(14) R. Guo, M. Decker, F. Setzpfandt, X. Gai, D.-Y. Choi, R. Kiselev, A. Chipouline, I. Staude, T. Pertsch, D. N. Neshev and Y. S. Kivshar, Sci. Adv., 2017, 3, e1700007.
(15) Z. Li, E. Palacios, S. Butun and K. Aydin, Nano Lett., 2015, 15, 1615.
(16) Y. Zhang, L. Zhou, J.-Q. Li, Q.-J. Wang and C.-P. Huang, Sci. Rep., 2015, 5, 10119.
(17) S. Gao, W. Yue, C.-S. Park, S.-S. Lee, E.-S. Kim and D.-Y. Choi, ACS Photonics, 2017, 4, 322.
(18) L. Zhang, J. Hao, M. Qiu, S. Zouhdi, J. K. W. Yang and C.-W. Qiu, Nanoscale, 2014, 6, 12303.
(19) Z. Li, E. Palacios, S. Butun and K. Aydin, Adv. Opt. Mater., 2016, 4, 953.
(20) F. Lütolf, M. Stalder and O. J. F. Martin, Opt. Lett., 2014, 39, 6557.
(21) Y. Huang, Q. Zhao, S. K. Kalyoncu, R. Torun, Y. Lu, F, Capolino and O. Boyraz, Appl. Phys. Lett., 2014, 104, 161106.
(22) M. Pu, X. Li, X. Ma, Y. Wang, Z. Zhao, C. Wang, C. Hu, P. Gao, C. Huang, H. Ren, X. Li, F. Qin, J. Yang, M. Gu, M. Hong and X. Luo, Sci. Adv., 2015, 1, e1500396.
(23) Y. Z. Ho, B. H. Cheng, W. L. Hsu, C. M. Wang and D. P. Tsai, Appl. Phys. Express, 2016, 9, 072502.
(24) N. M. Estakhri and A. Alù, J. Opt. Soc. Am. B, 2016, 33, A21.
(25) J. Hu, C.-H. Liu, X. Ren, L. J. Lauhon and T. W. Odom, ACS Nano, 2016, 10, 10275.
(26) A. Forouzmand and H. Mosallaei, J. Nanophoton., 2017, 11, 010501.
(27) D. Wen, F. Yue, G. Li, G. Zheng, K. Chan, S. Chen, M. Chen, K. F. Li, P. W. Wong, K. W. Cheah, E. Yue Bun Pun, S. Zhang and X. Chen, Nat. Commun., 2015, 6, 8241.
(28) X. Li, L. Chen, Y. Li, X. Zhang, M. Pu, Z. Zhao, X. Ma, Y. Wang, M. Hong and X. Luo, Sci. Adv., 2016, 2, e1601102.
(29) Y. Cui, K. H. Fung, J. Xu, H. Ma, Y. Jin, S. He, N. X. Fang, Nano Lett., 2012, 12, 1443.
(30) M. Lobet, M. Lard, M. Sarrazin, O. Deparis and L. Henrard, Opt. Express, 2014, 22, 12678.
(31) C. Pfeiffer and A. Grbic, Appl. Phys. Lett., 2013, 102, 231116.

(32) C. Pfeiffer, N. K. Emani, A. M. Shaltout, A. Boltasseva, V. M. Shalaev, and A. Grbic, Nano Lett., 2014, 14, 2491.
(33) A. Arbabi, E. Arbabi, Y. Horie, S. M. Kamali and A. Faraon, Nat. Photon., 2017, 11, 415.
(34) A. Arbabi, E. Arbabi, S. M. Kamali, Y. Horie, S. Han and A. Faraon, Nat. Commun., 2016, 7, 13682.
(35) Z. Lin, B. Groever, F. Capasso, A. W. Rodriguez and M. Lončar, 2017, arXiv:1706.06715.
(36) W. Ma, Z. Huang, X. Bai, P. Zhan and Y. Liu, ACS Photonics, 2017, 4, 1770.
(37) M. Pu, Z. Zhao, Y. Wang, X. Li, X. Ma, C. Hu, C. Wang, C. Huang and X. Luo, Sci. Rep., 2015, 5, 9822.
(38) J. Cheng and H. Mosallaei, J. Opt. Soc. Am. B, 2015, 32, 2115.
(39) G. Zheng, H. Mühlenbernd, M. Kenney, G. Li, T. Zentgraf and S. Zhang, Nat. Nanotechnol., 2015, 10, 308-312.
(40) V. R. Shrestha, S.-S. Lee, E.-S. Kim and D.-Y. Choi, Nano Lett., 2014, 14, 6672.
(41) S. Larouche, Y.-J. Tsai, T. Tyler, N. M. Jokerst and D. R. Smith, Nat. Mater., 2012, 11, 450.
(42) A. Pors, O. Albrektsen, I. P. Radko and S. I. Bozhevolnyi, Sci. Rep., 2013, 3, 2155.
(43) Y. Zhang, J.-Z. Zhu and C.-P. Huang, Phys. Lett. A, 2016, 380, 3949.
(44) L. Huang, X. Chen, H. Mühlenbernd, G. Li, B. Bai, Q. Tan, G. Jin, T. Zentgraf and S. Zhang, Nano Lett., 2012, 12, 5750.
(45) Lumerical Solutions Inc., "FDTD Solutions," https://www.lumerical.com/tcad-products/fdtd/.
(46) E. Khaidarov, H. Hao, R. Paniagua-Domínguez, Y. F. Yu, Y. H. Fu, V. Valuckas, S. L. K. Yap, Y. T. Toh, J. S. K. Ng and A. I. Kuznetsov, Nano Lett., 2017, 17, 6267.
(47) D. Sell, J. Yang, S. Doshay, R. Yang and J. A. Fan, Nano Lett., 2017, 17, 3752.
(48) D. Lin, M. Melli, E. Poliakov, P. St. Hilaire, S. Dhuey, C. Peroz, S. Cabrini, M. Brongersma and M. Klug, Sci. Rep., 2017, 7, 2286.
(49) V. S. Asadchy, A. Wickberg, A. Díaz-Rubio and M. Wegener, ACS Photonics, 2017, 4, 1264.
(50) A. Díaz-Rubio, V. S. Asadchy, A. Elsakka and S. A. Tretyakov, Sci. Adv., 2017, 3, e1602714.
(51) A. Pors and S. I. Bozhevolnyi, Opt. Express, 2013, 21, 27438.
(52) E. G. Loewen and E. Popov, Diffraction Gratings and Applications, CRC Press, New York, 1997.
(53) T. P. Xiao, O. S. Cifci, S. Bhargava, H. Chen, T. Gissibl, W. Zhou, H. Giessen, K. C., Jr. Toussaint, E. Yablonovitch and P. V. Braun, ACS Photonics, 2016, 3, 886.
(54) C. Yan, K.-Y. Yang and O. J. F. Martin, Light Sci. Appl., 2017, 6, e17017.

Figures and captions:

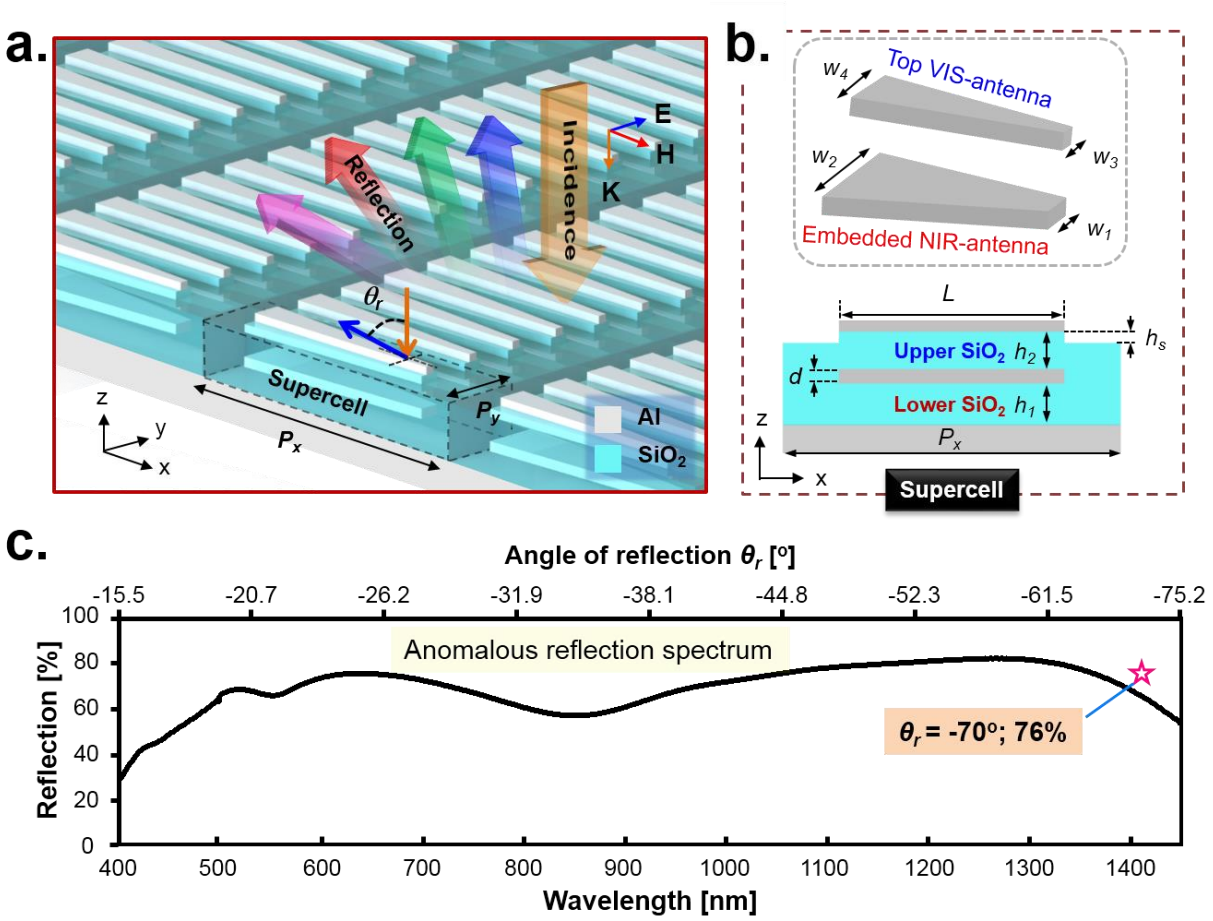

Fig. 1 (a) Schematic configuration of the proposed vertically integrated visible and near-infrared metasurfaces. (b) The elemental supercell of the metasurface incorporates two vertically integrated Al trapezoidal antennae with unequal lateral dimension. For the supercell, the pitches are P_x = 1500 nm and P_y = 250 nm, while the thickness and length of the two antennae are d = 40 nm and L = 1000 nm, respectively. The top VIS-antenna in the shape of a trapezoid exhibit base widths of w_3 = 40 nm and w_4 = 130 nm, while the embedded-NIR case has base widths of w_1 = 90 nm and w_2 =250 nm. The thicknesses of the lower and upper SiO_2 layers are h_1 = 90 nm and h_2 = 90 nm, respectively. The thickness of the SiO_2 step beneath the top VIS-antenna is h_s = 40 nm. (c) The anomalous reflection corresponding to the -1st order diffraction has been calculated for the proposed metasurface. The deflection efficiency is observed to peak at 76% at an angle of -70° under the condition of no loss, as marked by the star symbol on the chart. The relationship between the wavelength and the angle of anomalous reflection θ_r is also plotted.

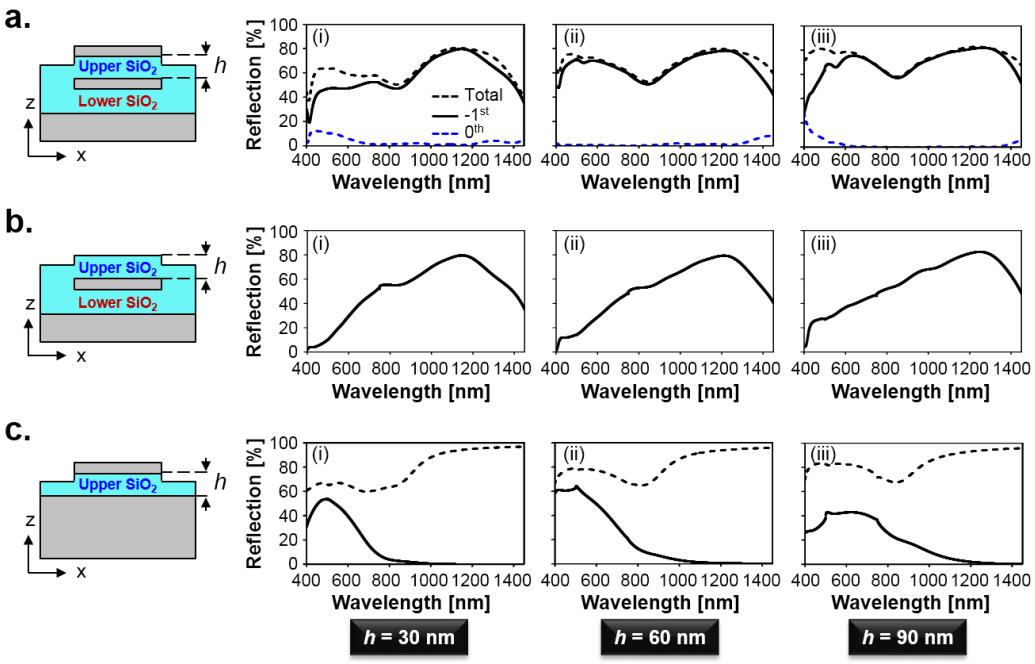

Fig. 2 Simulated -1[st] order diffraction spectra (in solid black lines) for the cases of (a) the proposed metasurface adopting both a top VIS-antenna and an embedded NIR-antenna, (b) a metasurface with an embedded NIR-antenna alone, and (c) a metasurface with a top VIS-antenna alone. For each case, the black and blue dashed lines represent the spectral characteristics for the total reflection and the zeroth-order diffraction, respectively. The upper SiO_2 is considered to have thicknesses of (i) h = 30 nm, (ii) h = 60 nm, and (iii) h = 90 nm.

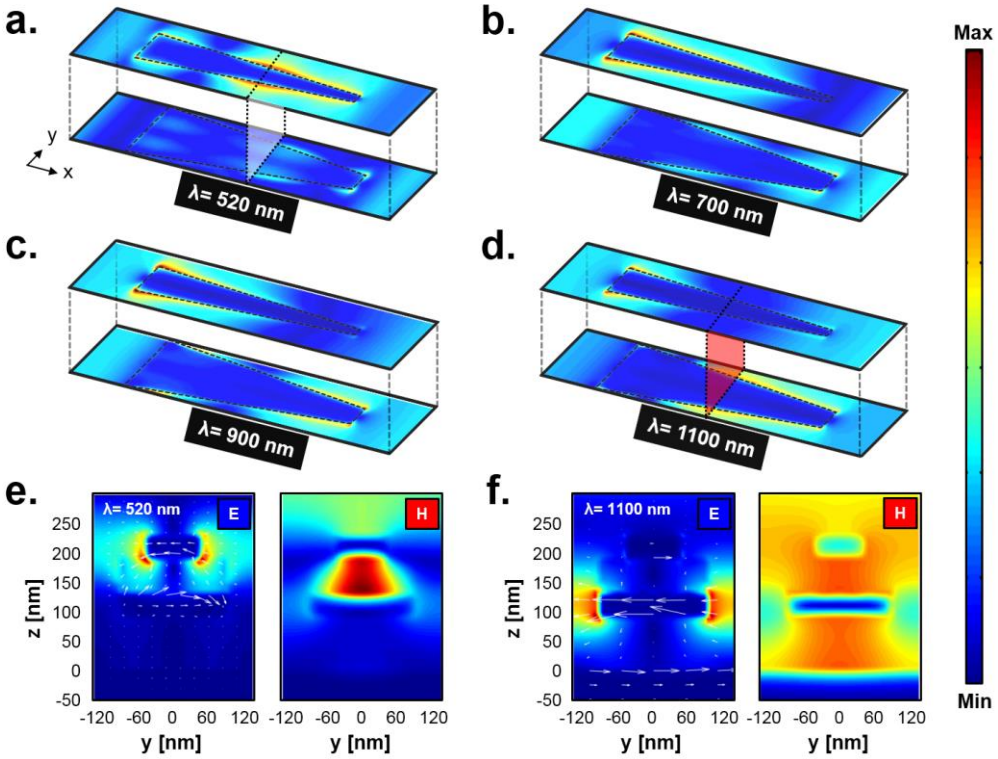

Fig. 3 Simulated total electric field distributions on the surface of the top VIS-antenna and the embedded NIR-antenna at the wavelengths of (a) 520 nm, (b) 700 nm, (c) 900 nm, and (d) 1100 nm, for the integrated metasurface with an upper SiO_2 layer of 60-nm thickness. The electric (E) and magnetic (H) field profiles on the designated cross-sectional planes are inspected for two representative wavelengths of (e) 520 nm and (f) 1100 nm.

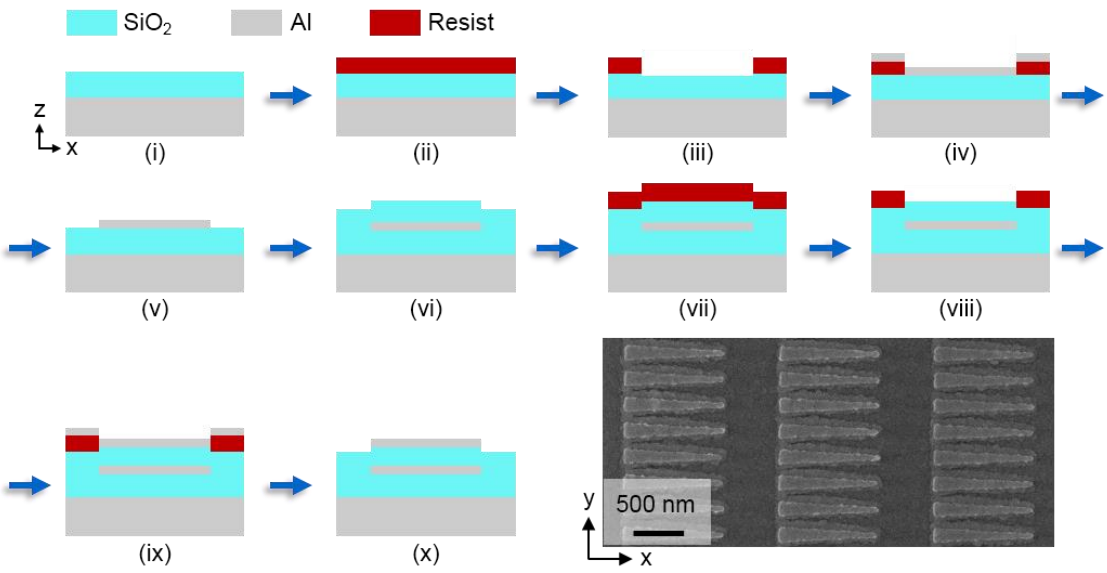

Fig. 4 Flow chart illustrating the fabrication procedure for the designed metasurface. Inset at the bottom right shows the SEM image of the completed device.

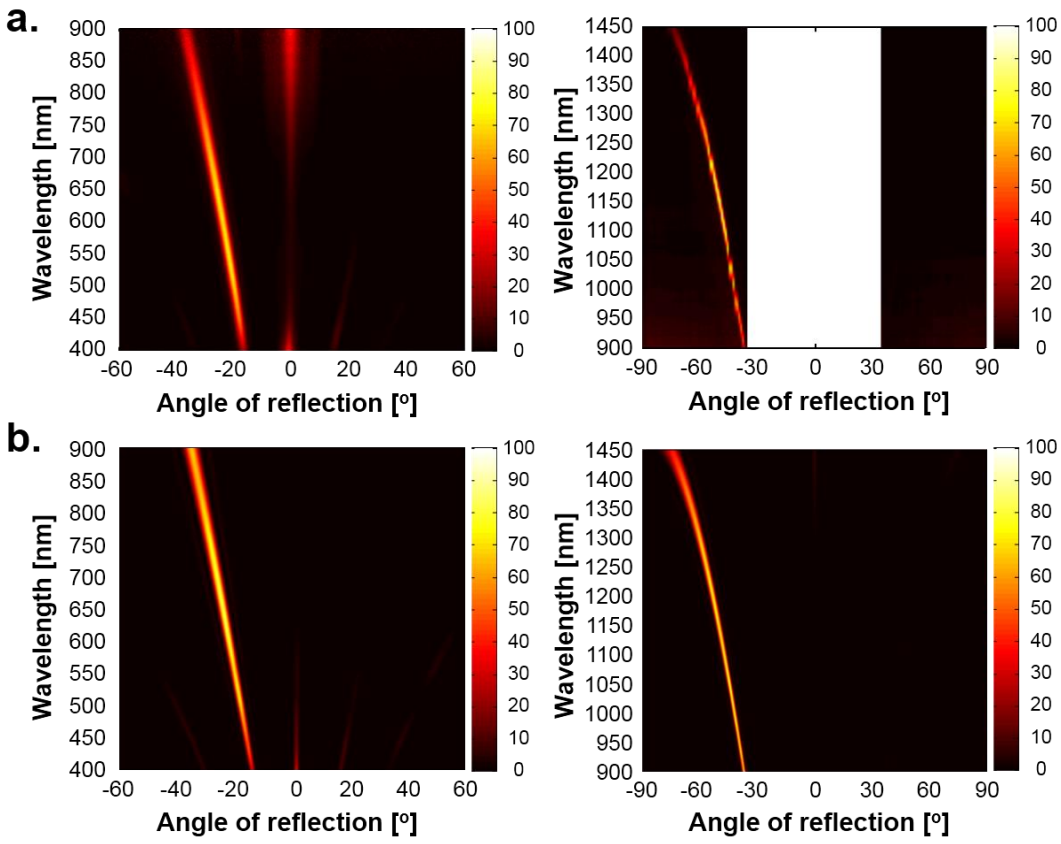

Fig. 5 Far-field intensity profile as a function of the wavelength and reflection angle in (a) measurement, and (b) simulation.

Table of Contents Graphic